3B2v8.06a/w (Dec 5 2003).51c + model | MAGMA : 53015 | Prod.Type:FTP pp.1–7(col.fig.:NIL) | ED:AjeeshVV PAGN:Jay SCAN:

ARTICLE IN PRESS

Available online at www.sciencedirect.com

SCIENCE DIRECT

ELSEVIER

Journal of Magnetism and Magnetic Materials ▮ (▮▮▮▮) ▮▮▮–▮▮▮

Journal of magnetism and magnetic materials

www.elsevier.com/locate/jmmm

Magnetic and transport properties of $RCoIn_5$ (R = Pr, Nd) and $RCoGa_5$ (R = Tb–Tm)

J. Hudis[a], R. Hu[b,c], C.L. Broholm[a], V.F. Mitrović[c], C. Petrovic[b,*]

[a]*Department of Physics and Astronomy, Johns Hopkins University, Baltimore, MD 21218, USA*
[b]*Condensed Matter Physics and Materials Science Department, Brookhaven National Laboratory, Upton, NY 11973, USA*
[c]*Physics Department, Brown University, Providence, RI 02912, USA*

Received 15 February 2006; received in revised form 25 March 2006

Abstract

We report on magnetic and transport properties of single crystals of the light rare earth containing series of compounds $RCoIn_5$ (R = Pr, Nd) and heavy rare earth containing series $RCoGa_5$ (R = Tb–Tm). All the compounds crystallize in the tetragonal $HoCoGa_5$ crystal structure and are very good metals with small defect scattering at low temperatures. $NdCoIn_5$ and members of the $RCoGa_5$ series with large de Gennes factors order antiferromagnetically.

Keywords: Crystal growth; Magnetic anisotropy

0. Introduction

Magnetism and superconductivity are the two major cooperative phenomena in condensed matter physics and the relationship between them has been studied extensively in recent years. Magnetic fluctuations present in many heavy fermion systems have been proposed to mediate and give rise to unconventional Cooper pairing [1,2]. A recently discovered family of 115 $CeMIn_5$ and $PuCoGa_5$ superconductors [3–6] with easily tunable ground states has considerably advanced our knowledge of the interplay between superconductivity and magnetism in heavy fermion systems [7]. The magnetic interaction model may be relevant for Cooper pairing in heavy fermion metallic systems close to a magnetic instability [8,9]. Besides all 115 systems, other examples of inter-metallics with competing magnetic and superconducting order parameters include $CePt_3Si$ [10], $CeCu_2Si_2$ [11] and a variety of pressure-induced superconductors that crystallize in $ThCr_2Si_2$ crystal structure, $CeIn_3$ [12], as well as several uranium-based materials including UGe_2 [13], URhGe [14], UBe_{13} [15], UPd_2Al_3 [16], UNi_2Al_3 [17] and UPt_3 [18]. Since electronic and magnetic anisotropy are important parameters in this, it is of interest to study magnetic interactions in the parent $HoCoGa_5$ crystal structure. In this paper we have outlined magnetic interactions of isostructural and non-hybridizing local moment-bearing counterparts of $CeMIn_5$ and $PuCoGa_5$: the $RCoIn_5$ (R = Pr, Nd) [19] and the $RCoGa_5$ (R = Tb–Tm) series. The successful growth of high-quality single crystals of the light rare-earth 115's with In and heavy rare-earth 115's with Ga has allowed us to address the evolution of anisotropic magnetic properties within the series with the change of rare earth as well as the occurrence and temperature dependence of metamagnetic transitions.

1. Experimental details

Large single crystals were grown out of indium flux [20–22]. The crystals grew as plates with the *c*-axis perpendicular to the plate. The typical crystal size for $RCoIn_5$ was up to $(10 \times 10 \times 1)\,mm^3$ for R = Pr whereas the typical R = Nd plate surface area was 2–5 times smaller. Crystals of $RCoGa_5$ grew as thicker plates for all R = Tb–Tm. We were unable to grow the $RCoGa_5$ phase under the same synthesis conditions for R = Gd and Yb.

*Corresponding author. Tel.: +1 631 344 5065; fax: +1 631 344 2739.
E-mail address: petrovic@bnl.gov (C. Petrovic).

0304-8853/$ - see front matter © 2006 Published by Elsevier B.V.
doi:10.1016/j.jmmm.2006.04.023

Attempts to grow Gd and Yb members of the series gave $GdIn_3$ and $YbCo_2Ga_8$ phases. Powder X-ray patterns were taken at room temperature using Rigaku Miniflex with CuK_α radiation. The data were collected using 2θ scan in the range from 10–90°. Single crystals were thoroughly ground to a fine powder. Le Bail unit cell refinements were performed using Rietica software. Magnetization measurements were performed using a commercial Quantum Design MPMS XL 7 magnetometer. Temperature sweeps were performed on warming, after zero-field cooling to 1.7 K and applying a field of 1 kOe. The samples were manually aligned to measure the magnetization along the appropriate axis. Polycrystalline averages were calculated as $\chi(T) = [2\chi_{ab}(T) + \chi_c(T)/3]$ and were used to obtain the high-temperature effective moments. Temperature-dependent magnetic susceptibility M/H curves were fit to Curie–Weiss (CW) law at high temperatures (100–350) K, with and without a temperature independent Pauli (χ_0) term: $\chi(T) = \chi_0 + \chi$ (CW). The temperature-independent term χ_0 includes contributions of Pauli $\chi_P = \mu_B^2 N(E_F)$ paramagnetic susceptibility (where $N(E_F)$ represents the electronic density of states at the Fermi level), core and Landau diamagnetism. The CW term $\chi(T) = C/(T - \Theta)$ reflects the contribution of localized moments where C is the Curie constant and Θ is the Weiss temperature. We have found that for all investigated materials the Pauli susceptibility was negligible except for $TbCoGa_5$. The temperatures at which $\partial(\chi T)/\partial T$ and $\partial\rho/\partial T$ have maxima are quoted as experimental values for the Neel temperature [23,24]. The in-plane resistance was measured using a Linear Research LR 700 AC bridge with a frequency of 16 Hz in the (H, T) environment of Quantum Design MPMS XL 7 ($RCoIn_5$) and in a home built resistance apparatus using a DC current source and a displex closed cycle cryostat down to 15 K ($RCoGa_5$). Electrical contacts were made with Epotek-H20E silver epoxy. DC current polarity was alternated and 1 mA currents were used. Excess In and Ga was removed from the surface of samples by a combination of mechanical polishing and etching in diluted HCl for several hours followed by thorough rinsing in ethanol. No samples obtained through this process showed signs of free indium contamination which would be reflected by a resistance drop at the superconducting temperature of indium ($T_C = 3.4$ K). There is uncertainty in absolute resistivity values associated with the sample geometry due to the uneven surfaces of etched samples. We measured several samples for each concentration in order to reduce measurement error. This also allowed us to estimate uncertainties in absolute values. The dimensions of the samples were measured by a high-precision optical microscope Nikon SMZ-800 with 10 μm resolution and average values are presented. Randomly chosen samples within each batch had consistent $R(T)$ curves.

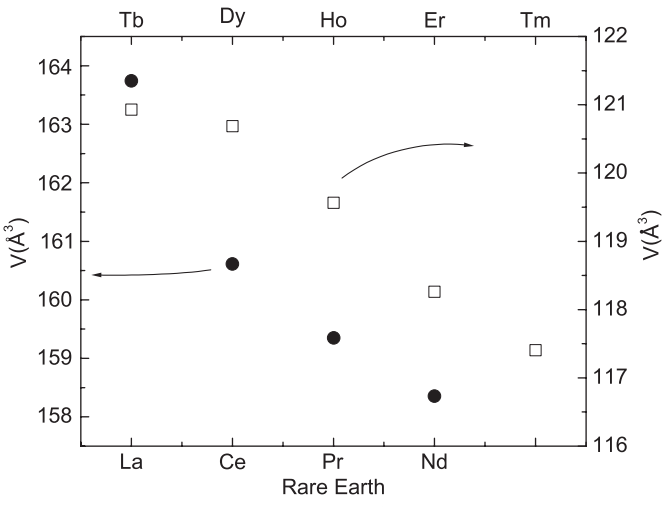

Fig. 1. Lattice parameters of $RCoIn_5$ (R = Pr, Nd) (•) and $RCoGa_5$ (R = Tm−Tb) (□) as a function of rare earth.

2. Crystal structure

The X-ray patterns were consistent with the tetragonal $HoCoGa_5$ structure (P4/mmm) [25]. All peaks were indexed and no impurity phases were detected. The unit cell volume for light rare-earth members of the $RCoIn_5$ series and for heavy members of the $RCoGa_5$ series is shown in Fig. 1. The individual lattice parameters are shown in Table 1. We see a smooth evolution of the unit cell volume and no deviation from the usual lanthanide contraction.

3. $RCoIn_5$ (R = Pr, Nd)

Magnetization measurements show that $PrCoIn_5$ is a CW paramagnet at high temperatures (Fig. 2). By fitting the polycrystalline average of the inverse susceptibility above 150 K to the CW law we get an effective moment of $(3.4 \pm 0.1)\mu_B$ per Pr^{3+} and a Weiss temperature of −21(1) K. Anisotropic Weiss temperatures are −43(1) K for H parallel to c and +19(1) K for H parallel to a-axis. No magnetic ordering is observed for $PrCoIn_5$ for $T > 1.7$ K (Fig. 2 inset). Fig. 2 also shows the inverse susceptibility of $NdCoIn_5$. Fitting the polycrystalline average to the CW law gives an effective moment of $(3.7 \pm 0.1)\mu_B$ per Nd^{3+} and a Weiss temperature of $\Theta_{poly} = -22(1)$ K. Anisotropic Weiss paramagnetic temperatures are $\Theta_a = -35(2)$ K and $\Theta_c = +0.7(2)$ K. The low-temperature magnetic susceptibility is anisotropic (Fig. 2 inset) and there are signatures of magnetic ordering at 8 K in a field of 1 kOe. An external magnetic field of 70 kOe shifts the peaks in magnetic susceptibility to 2.9 K, as expected for an antiferromagnetic transition. Magnetic isotherms at $T = 1.7$ K (Fig. 3) show that for $PrCoIn_5$ the magnetization is linear for field applied along both crystalline axis, reaching only $0.65\,\mu_B/Pr^{3+}$ at 70 kOe for H parallel to c-axis. However, for $NdCoIn_5$ the magnetization isotherm for H parallel to c-axis shows a metamag-

Table 1
Structural and magnetic properties of $RCoIn_5$ (R = Pr, Nd) and $RCoGa_5$ (R = Tb−Tm) compounds

	a (Å)	c (Å)	Θ_a (K)	Θ_c (K)	P_{eff} (μ_B)	θ_{ave} (K)	T_N (K)	α_J ($\times 10^2$)
$PrCoIn_5$	4.5987(2)	7.5339(4)	−43(1)	+19(1)	3.4(1)	−21(1)	—	−1.05
$NdCoIn_5$	4.5913(2)	7.5127(5)	−35(2)	+0.7(2)	3.7(1)	−22(1)	8.0	−0.643
$TbCoGa_5$	4.2140(6)	6.8100(5)	−71(1)	−43(9)	9.9(2)	−62(3)	36.0	−1.01
$DyCoGa_5$	4.2157(2)	6.7930(6)	−60(2)	+14(2)	10.3(1)	−24(1)	25.0	−0.635
$HoCoGa_5$	4.1992(1)	6.7807(3)	−27(1)	+4(1)	10.0(6)	−16(2)	9.5	−0.222
$ErCoGa_5$	4.1845(2)	6.7539(4)	−1(7)	−19(8)	9.1(1)	−6(5)	—	+0.254
$TmCoGa_5$	4.1780(1)	6.7276(3)	+9(1)	−51(1)	7.4(1)	−4(1)	—	+1.01

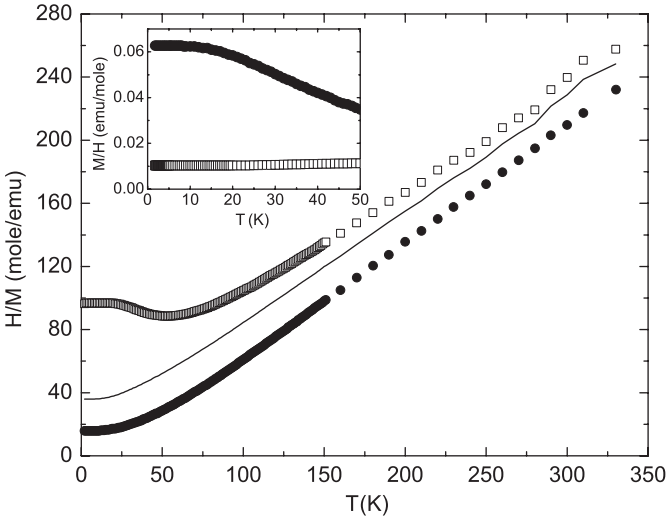

Fig. 2. Temperature-dependent inverse susceptibility H/M of $PrCoIn_5$ for $H \| a$-axis (□), $H \| c$-axis (•) and polycrystalline average (line). The inset shows anisotropic low-temperature magnetic susceptibility (M/H).

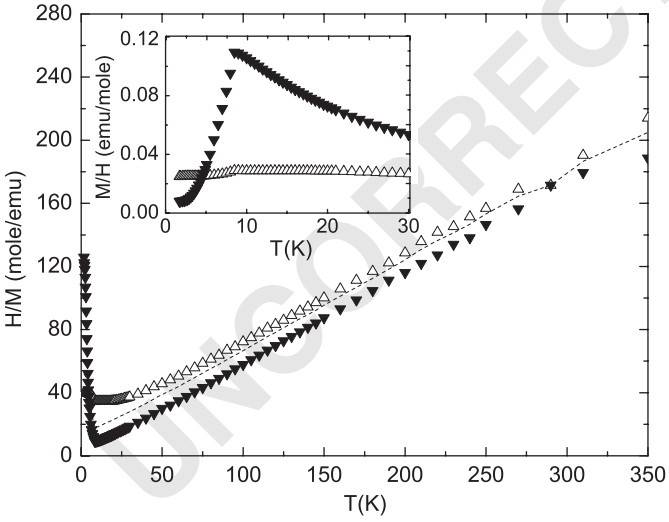

Fig. 3. Temperature-dependent inverse susceptibility H/M of $NdCoIn_5$ for $H \| a$ axis (△), $H \| c$-axis (▼) and polycrystalline average (dashed line). The inset shows anisotropic low-temperature magnetic susceptibility (M/H).

netic transition. The maximum magnetization measured was 1.3 μ_B which is lower than the saturated moment of the free Nd^{3+} ion. A full metamagnetic phase diagram may be obtained by measuring the angular dependence of magnetization in higher fields and by high-field neutron diffraction measurements.

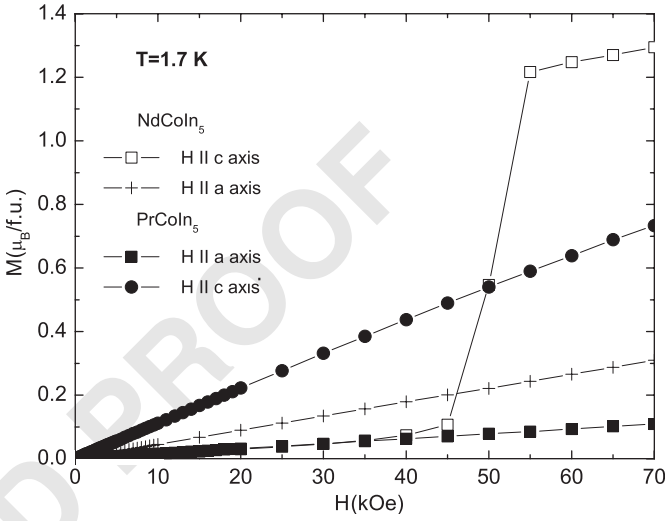

Fig. 4. Field-dependent magnetization for $PrCoIn_5$ and $NdCoIn_5$.

The electrical resistivity data for $RCoIn_5$ with R = Pr, Nd are shown in Fig. 4. For both compounds the resistivity decreases with decreasing temperature as expected for a metal. For $NdCoIn_5$ there is a distinct loss of spin disorder scattering at the antiferromagnetic phase transition T_N = 8 K (Fig. 4 inset). The very small residual resistivities for $PrCoIn_5$ (0.1 μΩ cm) and $NdCoIn_5$ (0.22 μΩ cm) indicate a high level of crystalline order and very weak defect scattering. The high-temperature resistivity is dominated by spin disorder scattering and the resistivity values for R = Nd are higher, as expected due to the larger de Gennes factor. The metamagnetic transition around 45 kOe in $NdCoIn_5$ manifests itself not only in the field dependent magnetization but also through anomalies in the field dependent magnetoresistance (Fig. 4 inset). The metamagnetic transition in $NdCoIn_5$ is seen at lower field (40 kOe) in magnetoresistance than in magnetization (50 kOe), indicating possible sample misalignment and magnetic anisotropy. Angular-dependent magnetization measurements would be useful to clarify this issue.

4. $RCoGa_5$ (R = Tb−Tm)

Both $TbCoGa_5$ and $DyCoGa_5$ order antiferromagnetically (Fig. 5). Whereas $TbCoGa_5$ shows very weak anisotropy in its paramagnetic state and in its ordered state, the magnetic properties of $DyCoGa_5$ are strongly anisotropic in its ordered state, with the local Dy^{3+} moments constrained along the c-axis of the crystal. The polycrystalline average of the inverse susceptibility gives effective moments of $9.9(2)\,\mu_B/Tb^{3+}$ and $10.3(1)\,\mu_B/Dy^{3+}$ and $\Theta_{ave} = -62(3)$ K and $\Theta_{ave} = -24(1)$ K for $TbCoGa_5$ and $DyCoGa_5$, respectively. Fit to anisotropic Weiss susceptibility gives Weiss paramagnet temperatures Θ_a and Θ_c of $-71(1)$ and $-43(9)$ K for $TbCoGa_5$ and $-60(2)$ and $+14(2)$ K for $DyCoGa_5$. The anomalously large temperature-independent term (usually dominated by Pauli susceptibility in rare-earth intermetallics) for $TbCoGa_5$ was 0.021(7) emu/mol. Since $TbCoGa_5$ lies at the border of the structure formation of $RCoGa_5$ series, it is possible that small crystal imperfections and/or vacancies influence band structure and Fermi level position in such way so that it contributes to larger Pauli paramagnetic term than in other investigated compounds. Below $T_N = 25$ K, $DyCoGa_5$ orders antiferromagnetically as determined by the maximum in $\partial(\chi T/\partial T)$. On the other hand, $TbCoGa_5$ shows two successive antiferromagnetic transitions at $T_{N1} = 36$ and $T_{N2} = 5$ K.

The magnetic behavior of $HoCoGa_5$, $ErCoGa_5$ and $TmCoGa_5$ single crystals is shown in Fig. 6. The inverse magnetic susceptibility H/M is CW-like at high temperatures, yielding high-temperature effective moments of 10.0(6), 9.1(1) and 7.4(1) μ_B and a polycrystalline average Weiss temperatures Θ_{ave} of $-16(2)$, $-6(5)$ and $-4(1)$ K, respectively. A fit to an anisotropic Weiss susceptibility gives Weiss paramagnet temperatures Θ_a and Θ_c of $-27(1)$ and $+4(1)$ K for $HoCoGa_5$, $-1(7)$ and $-19(8)$ K for $ErCoGa_5$ and $+9(1)$ and $-51(1)$ K for $TmCoGa_5$. There is no sign of magnetic order for $ErCoGa_5$ and $TmCoGa_5$ for $T \gtrsim 2$ K. $HoCoGa_5$ orders magnetically at $T_N = 9.5$ K (Fig. 7 inset).

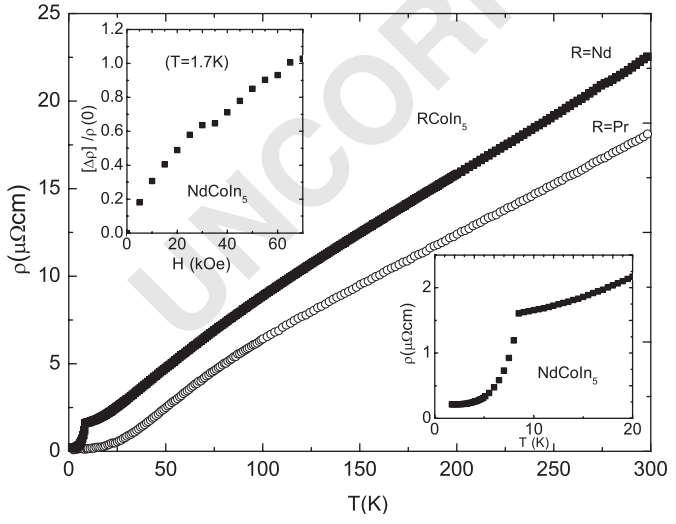

Fig. 5. Resistivity of $RCoIn_5$ (R = Pr, Nd). Insets show low-temperature resistivity of $NdCoIn_5$ and field-dependent magnetoresistance $\Delta\rho = \rho(H)/\rho(0)$.

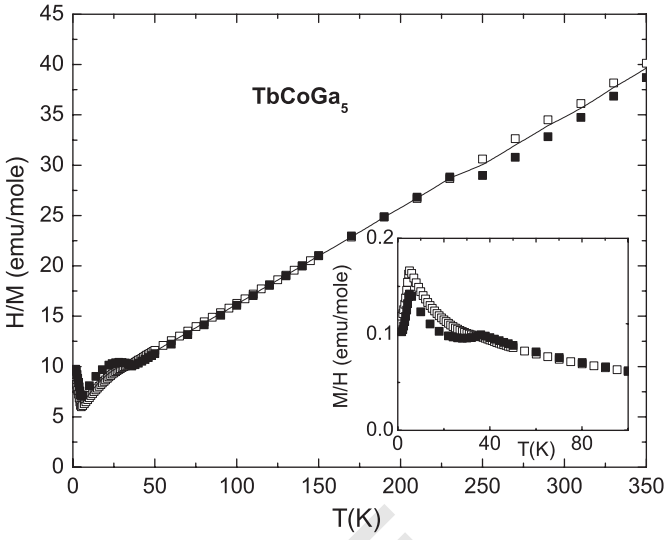

Fig. 6. Temperature-dependent inverse susceptibility H/M of $TbCoGa_5$ in an applied field of 1 kOe for $H\|a$-axis (□) and $H\|c$-axis (■). Inset shows low-temperature magnetic susceptibility M/H. Solid line shows polycrystalline average.

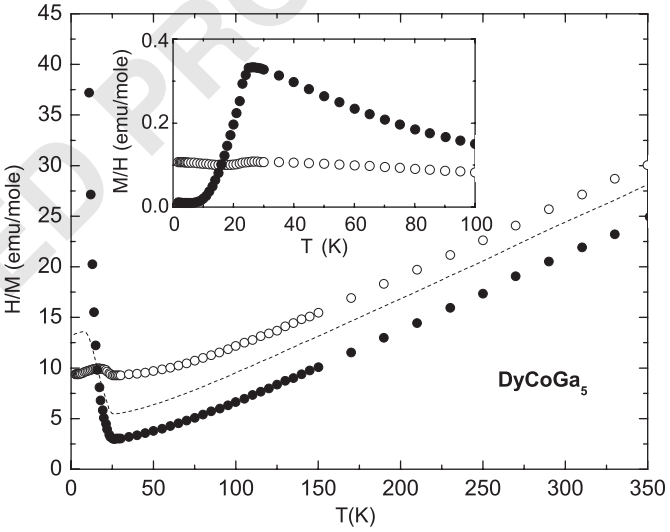

Fig. 7. Temperature-dependent inverse susceptibility H/M of $DyCoGa_5$ in an applied field of 1 kOe for $H\|a$-axis (○) and $H\|c$-axis (●). Inset shows low-temperature magnetic susceptibility M/H. Dashed line shows polycrystalline average.

The electrical resistivity data for $RCoGa_5$ (R = Tb−Tm) are shown in Fig. 8. In all cases, the resistivity has a metallic temperature dependence, decreasing with decreasing temperature. For the magnetically ordered rare earths we observe a loss of spin disorder scattering at the antiferromagnetic ordering temperatures and values of T_C estimated from $\partial\rho/\partial T$ are in good agreement with values estimated from the $(\partial\chi T/\partial T)$. All compounds have very small residual resistivity values, and $\rho(300\,K)/\rho(15\,K) \approx 10$

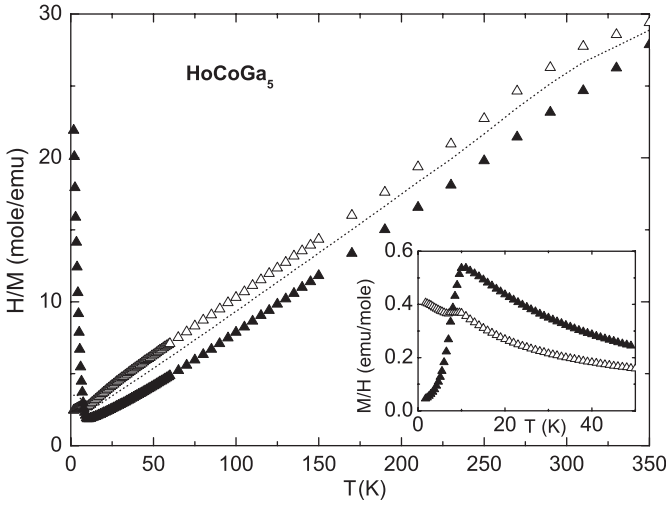

Fig. 8. Temperature-dependent inverse susceptibility H/M of $HoCoGa_5$ in an applied field of 1 kOe for $H\|a$-axis (△) and $H\|c$-axis (▲). Inset shows low-temperature magnetic susceptibility M/H. Dotted line shows polycrystalline average.

for all measured samples, indicating small amounts of defects and disorder scattering at low temperatures. The resistivity values are generally larger for materials with a larger de Gennes factor.

5. Discussion

We have presented the first data for the magnetic and transport properties of the $RCoIn_5$ (R = Pr, Nd) and $RCoGa_5$ (R = Tb−Tm) series. A large resistivity ratio and small residual resistivity values confirm a high degree of crystalline order.

The high-temperature magnetism of both series is local moment-like in displaying CW behavior with effective magnetic moments approach with free ion values. Table 1 shows summary of the magnetic properties. For $H\|a$, the CW temperatures Θ_a are negative for all compounds except $TmCoGa_5$. The c-axis CW temperatures Θ_c, however, are positive for both Pr and Nd members of $RCoIn_5$ series as well as for Dy and Ho members of the $RCoGa_5$ series. While the interactions are predominantly antiferromagnetic as indicated by the negative polycrystalline averaged CW temperatures, there is considerable spin space anisotropy as anticipated for rare-earth ions with strong spin-orbit coupling.

The magnetic interactions among localized rare-earth magnetic moments in a metallic environment are generally described within the framework of Rudermann–Kittel–Kasuya–Yosida (RKKY) theory of indirect exchange via conduction electrons. Not considering the sometimes intricate effects of competing interactions, the magnetic ordering temperature in the rare-earth series is correspondingly approximated [26] by

$$T_M \approx 8N(E_F)/k_B I^2 DG, \quad (1)$$

where $N(E_F)$ is the conduction electron density of states at the Fermi level, k_B is the Boltzman constant, I and J are an exchange interaction parameter and the total angular momentum quantum number of the rare-earth ion, $DG = (g_J - 1)2J(J+1)$ is the de Gennes factor and g_J is the Lande g factor. The CW temperature Θ_{ave} derived from the polycrystalline average should scale with the de Gennes factor since it is also proportional to indirect interactions with local moments. Fig. 9 shows that though magnetic ordering temperatures T_N and $|\Theta_{ave}|$ seem to roughly increase with the de Gennes factor in the $RCoGa_5$ (R = Tb−Tm) series, quite significant deviations are possible. Degree of deviations from line connecting DG = 0 point and magnetic ordering and CW temperatures of hypothetical $GdCoIn_5$ could further clarify this issue. Compounds with small values of the de Gennes factor do not order above 1.7 K. The determination of crystal field effects, carrier density and neutron diffraction measurements would certainly advance our understanding of magnetic interactions in this series.

The easy axis of magnetization in the paramagnetic state is c-axis in both $PrCoIn_5$ and $NdCoIn_5$ as well as for $RCoGa_5$ (R = Tb−Ho). This is reversed for R = Er and Tm, where the susceptibility is greater for fields applied in the tetragonal plane. The magnetic anisotropy arises from anisotropic exchange and CEF splitting of the Hund's rule multiplet due to the anisotropic coordination. The latter effect can be accounted for by a spin Hamiltonian, which for tetragonal point group symmetry takes the following form [27]:

$$H^{CEF} = B_2^0 O_2^0 + B_4^0 O_4^0 + B_4^4 O_4^4 + B_6^0 O_6^0 + B_6^4 O_6^4. \quad (2)$$

Here B_n^m are the Stevens coefficients that parametrize the anisotropy and O_n^m are Stevens operators. At high temperatures the B_2^0 term [28,29] can be the dominant term in the spin Hamiltonian with a larger effect on the uniform susceptibility than the exchange constant. In the

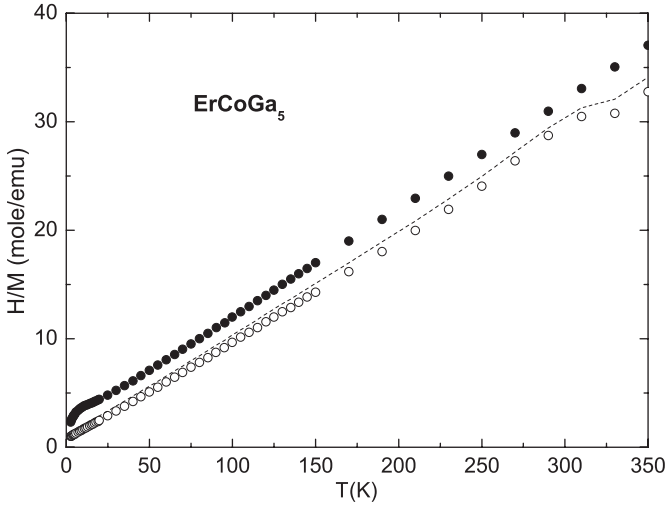

Fig. 9. Temperature-dependent inverse susceptibility H/M of $ErCoGa_5$ in an applied field of 1 kOe for $H\|a$-axis (○) and $H\|c$-axis (●). Dashed line shows polycrystalline average.

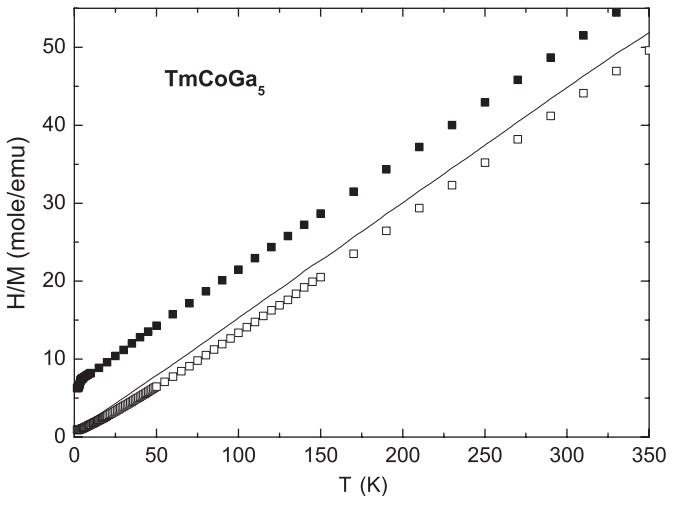

Fig. 10. Temperature-dependent inverse susceptibility H/M of $TmCoGa_5$ in an applied field of 1 kOe for $H\|a$-axis (□) and $H\|c$-axis (■). Solid line shows polycrystalline average.

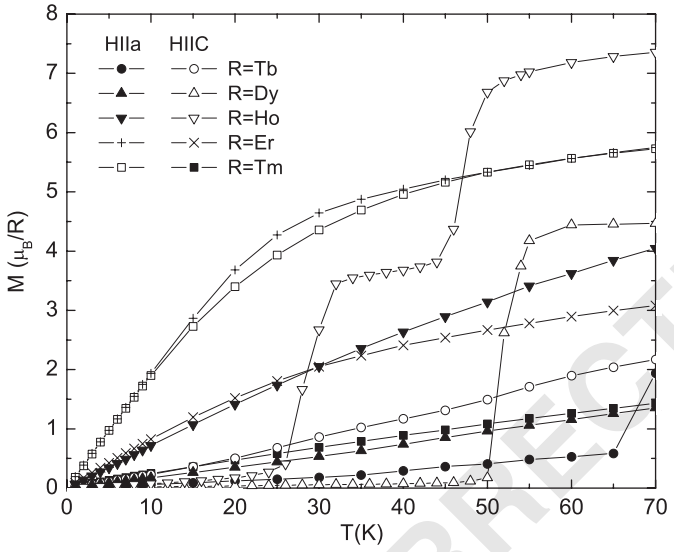

Fig. 11. Magnetization isotherms for $RCoGa_5$ compounds (R = Tb−Tm) at 1.7 K.

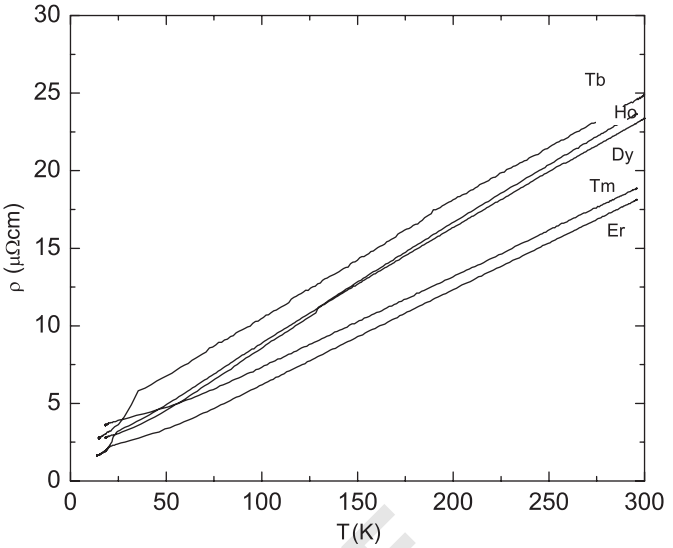

Fig. 12. The electrical resistivity of $RCoGa_5$ single crystals (R = Tb−Tm) for currents flowing parallel to a-axis of tetragonal $HoCoGa_5$ structure.

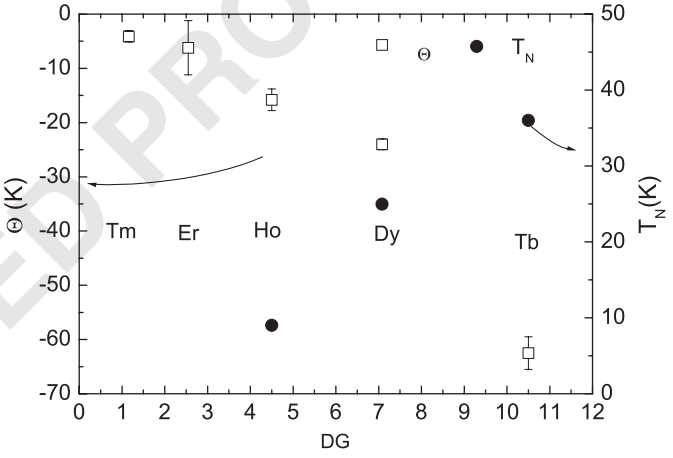

Fig. 13. Magnetic ordering temperatures and dependence of Curie–Weiss paramagnetic temperature Φ_{ave} on the de Gennes factor.

point charge model $B_2^0 = \langle r^2 \rangle A_2^0 \alpha_J$, where the expectation value of r^2 of 4f electron is always positive, α_J is a rare-earth-dependent multiplicative factor and A_2^0 is a geometrical factor which is constant in the series. Thus, the sign of B_2^0 depends exclusively on α_J whose values are listed in Table 1. The change in sign of this quantity shows that qualitatively the variation in anisotropy across the series is accounted for by the point charge model [30]. Specifically, for all $RCoIn_5$ and $RCoGa_5$ compounds that we examined. Negative values of α_J correspond to easy plane behavior while positive values are associated with easy axis anisotropy. The change in the easy axis of magnetization between $HoCoGa_5$ and $ErCoGa_5$ thus appears to be a consequence of the sign change of α_J (Figs. 10–12).

6. Summary

We have successfully synthesized single crystals of the $RCoIn_5$ (R = Pr, Nd) and the $RCoGa_5$ (R = Tb−Tm) series of rare-earth compounds and delineated their basic structural, magnetic and electronic transport properties. All compounds are metallic paramagnets or antiferromagnets, in some cases with rather anisotropic magnetism, which is most likely due to CEF splitting of the Hund's rule ground state multiplet. The RKKY model can account for the variation of the exchange interaction strength and ordering temperatures across the $RCoGa_5$ series for large values of the de Gennes factor (Fig 13). While the CW temperature extracted from susceptibility measurements along the c-direction is consistently positive for the $RCoIn_5$ series, it changes sign through the $RCoGa_5$ series. This contrasts with the negative (antiferromagnetic) value of the

CW temperature for fields in the basal plane and invites further work to understand the anisotropic magnetism of these high-quality metals.

Acknowledgments

We thank S.L. Bud'ko for useful comments. This work was carried out at the Brookhaven National Laboratory, which is operated for the US Department of Energy by Brookhaven Science Associates (DE-Ac02-98CH10886).

References

[1] G. Aeppli, A. Goldman, G. Shirane, E. Bucher, M.-Ch. Lux–Steiner, Phys. Rev. Lett. 58 (1987) 808.
[2] R. Joynt, L. Taillefer, Rev. Mod. Phys. 74 (2002) 235.
[3] C. Petrovic, P.G. Pagliuso, M.F. Hundley, R. Movshovich, J.L. Sarrao, J.D. Thompson, Z. Fisk, P. Monthoux, J. Phys. Condens. Matter 13 (2001) L337.
[4] C. Petrovic, R. Movshovich, M. Jaime, P.G. Pagliuso, M.F. Hundley, J.L. Sarrao, Z. Fisk, J.D. Thompson, Europhys. Lett. 53 (2001) 354.
[5] H. Hegger, C. Petrovic, E.G. Moshopolou, M.F. Hundley, J.L. Sarrao, Z. Fisk, J.D. Thompson, Phys. Rev. Lett. 84 (2000) 4986.
[6] J.L. Sarrao, L.A. Morales, J.L. Thompson, B.L. Scott, G.R. Stewart, F. Wastin, G. Rebizant, P. Boulet, E. Colineau, G.H. Lander, Nature 420 (2002) 297.
[7] N.J. Curro, T. Caldwell, E.D. Bauer, L.A. Morales, M.J. Graf, Y. Bang, A.V. Balatsky, J.D. Thompson, J.L. Sarrao, Nature 434 (2005) 622.
[8] P. Monthoux, G. Lonzarich, Phys. Rev. B 69 (2004) 064517.
[9] P. Monthoux, G. Lonzarich, Phys. Rev. B 66 (2002) 224504.
[10] E. Bauer, G. Hilscher, H. Michor, C. Paul, E.W. Scheidt, A. Gribanov, Y. Serogepin, H. Noel, M. Sigrist, P. Rogl, Phys. Rev. Lett 92 (2004) 027003.
[11] F. Steglich, J. Aarts, C.L. Bredl, W. Lieke, D. Meschede, W. Franz, H. Schafer, Phys. Rev. Lett. 43 (1979) 1892.
[12] N.D. Mathur, F.M. Grosche, S.R. Julian, I.R. Walker, D.M. Freye, R.K.W. Haselwimmer, G.G. Lonzarich, Nature 394 (1998) 39.
[13] S.S. Saxena, P. Agarwal, K. Ahilan, F.M. Grosche, R.K.W. Haselwimmer, M.J. Steiner, E. Pugh, I.R. Walker, S.R. Julian, P. Monthoux, G.G. Lonzarich, A. Huxley, I. Sheikin, D. Braithwaite, J. Flouquet, Nature 406 (2000) 587.
[14] D. Aoki, A. Huxley, E. Ressouche, D. Braithwaite, J. Flouquet, J.P. Brison, E. Lhotel, C. Paulsen, Nature 413 (2001) 613.
[15] H.R. Ott, H. Rudiger, Z. Fisk, J.L. Smith, Phys. Rev. Lett. 50 (1983) 1595.
[16] C. Geibel, C. Schank, S. Thies, H. Kitazawa, C.D. Bredl, A. Bohm, M. Rau, A. Grauel, R. Caspary, R. Helfrich, U. Ahlheim, G. Weber, F. Steglich, Z. Phys. B 84 (1991) 1.
[17] C. Geibel, S. Thies, D. Kaczorowski, D. Mehner, A. Grauel, B. Seidel, U. Ahlheim, R. Helfrich, K. Petersen, C.D. Bredl, F. Steglich, Z. Phys. B 83 (1991) 305.
[18] G.R. Stewart, Z. Fisk, J.O. Willis, J.L. Smith, Phys. Rev. Lett. 52 (1984) 679.
[19] N. Van Hieu, H. Shisido, A. Thamizhavel, R. Settai, S. Araki, Y. Nozue, T. Matsuda, Y. Haga, T. Takeuchi, H. Harima, Y. Onuki, J. Phys. Soc. Japan 74 (2005) 3320.
[20] Z. Fisk, J.P. Remeika, in: K.A. Gschneider, J. Eyring (Eds.), Handbook on the Physics and Chemistry of Rare Earths, vol. 12, Elsevier, Amsterdam, 1989.
[21] P.C. Canfield, Z. Fisk, Philos. Mag. B 65 (1992) 1117.
[22] P.C. Canfield, I.R. Fisher, J. Cryst. Growth 225 (2–4) (2001) 155.
[23] M.E. Fisher, Philos. Mag. 7 (1962) 1731.
[24] M.E. Fisher, J.S. Langer, Phys. Rev. Lett. 20 (1968) 665.
[25] Y.M. Kalychak, V.I. Zareba, V.M. Baranyak, V.A. Bruskov, P.Y. Zavalii, Russ. Metal. 1 (1989) 213.
[26] M.B. Maple, in: G.K. Shenoy, B.D. Dunlap, F.Y. Fradin (Eds.), Ternary Superconductors, North-Holland, Amsterdam, 1981, p. 131.
[27] J.L. Prather, U.S. International Bureau of Standards, Monograph No. 19.
[28] Y.L. Wang, Phys. Lett. A 35 (1971) 383.
[29] P. Boutron, Phys. Rev. B 7 (1973) 3226.
[30] M.T. Hutchings, in: F. Seits, D. Tumbull (Eds.), Advances in Research and Applications, Solid State Physics, vol. 16, Academic Press, New York, 1964.